

Hierarchical Segmentation of Vertebrae from X-ray Images

Gilberto Zamora*^a, Hamed Sari-Sarraf^a, Rodney Long^b

^aDepartment of Electrical and Computer Engineering, Texas Tech University, Lubbock, TX 79409

^bCommunications Engineering Branch, National Library of Medicine, Bethesda, MD 20894

ABSTRACT

The problem of vertebrae segmentation in digitized x-ray images is addressed with a hierarchical approach that combines three different methodologies. As a starting point, two customized active shape models are trained on data sets of cervical and lumbar images, respectively. Here, a methodology to include edge information in the gray-level modeling part of the active shape models is developed to increase the representativeness of the model and to improve the chances of finding vertebral boundaries. Active shape models' initialization shortcoming is then addressed by a customized implementation of the Generalized Hough Transform, which provides an estimate of the pose of the vertebrae within target images. Active shape models' shortcoming of lack of local deformation is addressed by a customized implementation of the technique of Deformable Models. In this implementation, an energy minimization approach is employed in which the external energy term is extracted from the training set of images and the internal energy terms control the shape of the template. Segmentation results on data sets of cervical and lumbar images show that the proposed hierarchical approach produces errors of less than 3mm in 75% of the cervical images and 6.4mm in 50% of the lumbar images.

Keywords: Image segmentation, hierarchical segmentation, x-ray images, GHT, ASM, DM.

1. Introduction

The problem of vertebrae segmentation in digitized x-ray images is of great importance for the assessment of vertebral abnormalities. The use of manual segmentation methods relies on subjective judgment and, thus, produces results that are neither accurate nor repeatable. Therefore, an automatic algorithm for segmenting vertebrae and for the subsequent assessment of vertebral abnormalities is of significant importance to the medical imaging community. However, current methodologies present a number of shortcomings that limit their success rate. The motivation of this work is to design, develop, and test an automatic segmentation algorithm that addresses such shortcomings and provides accurate segmentation with minimal human intervention. The selected approach is based on a hierarchical segmentation of vertebrae, which divides the process into three steps and each step performs a different level of segmentation from coarse to fine.

In our approach, we have selected the Generalized Hough Transform (GHT), Active Shape Models (ASM), and Deformable Models (DM) methodologies to develop a hierarchical segmentation algorithm. In GHT, a template, which represents the shape of the object of interest, is matched to a target image for different values of position, orientation, and scale. Therefore, the output of GHT is the pose of the object within the image. This pose can be used to initialize an ASM, extracted from a training set of x-ray images containing the vertebrae of interest. ASM is a technique that captures the variability of shape and local gray-level values from the training set of images and builds two models, one for shape (SM) and for gray-level values (GLM). Segmentation with ASM is achieved by iteratively deforming the SM towards the boundaries of the objects of interest as guided by GLM. Although ASM has been used in a variety of applications with reasonable success, it suffers from a number of well-known shortcomings. First, ASM requires an initialization step that places its initial shape close to the target object. Second, it requires GLM to be a good representative of the gray-level values of the images around the shapes of interest. And finally, the deformation of SM does not allow for local deformations of shape at key parts of the objects. We address the initialization shortcoming with GHT since it provides an estimate of the pose of the vertebrae. The local deformation shortcoming is addressed by building a number of DMs along the local shapes of interest, such as vertebral corners, and deforming them according to an energy minimization approach. In DM, the deformation is guided by external energy terms that pull the template towards boundaries, but is

constrained by internal energy terms that keep the shape of the template within predefined parameters. In our approach, we have customized the implementations of GHT, ASM, and DM to accommodate the distinctive characteristics of vertebrae in x-ray images.

In section 2, we describe some of the existing methodologies that address vertebrae segmentation. In section 3, we describe the proposed methodology for the hierarchical approach based on customized implementations of GHT, ASM, and DM. In section 4, the results of the segmentation on data sets of cervical and lumbar x-ray images are presented. Finally, section 5 presents our conclusions.

2. Assessment of vertebral shape

The assessment of vertebral shape for the detection of abnormalities can be divided into two categories: manual segmentation of vertebrae and semi-automatic and automatic segmentation of vertebrae. The distinction depends upon the degree of automation of the segmentation process.

2.1. Manual segmentation of vertebrae

In the clinical environment, there are two methods to manually segment vertebrae from x-ray images that are used by radiologists: Semiquantitative segmentation (SQ) and Quantitative Morphometry (QM). In both methods, visual evidence is combined with radiologists' experience in order to locate vertebrae. With these manual methods, radiologists are able to identify the different vertebral levels (cervical, thoracic, and lumbar) and assign labels that indicate specific shape characteristics. The degree of deformity is assigned through *flagging*; a numerical scale method in which degree 0 corresponds to normal shape and degree 3 corresponds to an extreme case of deformation [1,2,3]. Samples of types and degrees of deformation can be found in reference atlases [4].

In SQ, the radiologist, by looking at the spatial relationships between vertebrae, can identify which vertebrae are visible and the general pose and shape of the spine. Some of the information extracted from the images is: the shape of the vertebral endplates, which provides information about fractures; the separation between vertebrae, which is the main indicator of inter-vertebral disk anomalies; the shape of vertebral corners, which is used to assess the presence of osteophytes; and the alignment of the vertebrae, which indicates the presence of subluxation.

In QM, seven *morphometric points* are manually drawn on film. Of these points, four are placed at the corners of vertebrae, one is placed at the middle point of the superior endplate, one is placed at the middle point of the inferior endplate, and one is placed at the middle point of the anterior boundary [5]. Some radiologists also place eighth and ninth points when corner anomalies are detected as in the case of anterior osteophytes. QM is an important methodology for two reasons. First, once the morphometric points are placed on film, rulers and calipers are used to manually measure distances between points. These distances are employed to extract shape information that can be related to age, sex, race, and illness. Secondly, the spatial coordinates of morphometric points can be used as ground truth for semi-automatic and automatic segmentation methods that rely on a priori information about the shape of vertebrae.

2.2. Semi-automatic and automatic segmentation of vertebrae

Because SQ and QM are performed manually, they are time consuming, subjective, and often inaccurate. With the use of computer vision techniques, a number of different algorithms have been developed that perform some semi-automatic tasks that save time and produce acceptable estimates of vertebral shape. Semi-automatic and automatic segmentation methods can be divided into three major categories based on their basic principles as (1) empirical, (2) DM, and (3) statistical modeling.

Empirical methods for segmenting vertebrae use a priori knowledge of the anatomy of the spine and its surroundings. These methods rely on the visibility of these structures. Therefore, the possibility of success is limited by the information content on each analyzed image. Computer vision techniques involving pattern analysis [6], histogram manipulation [7], morphological operations [7,8], anatomy-based coordinate systems [9,10], and directional filtering [11] have been used

to locate and delineate vertebrae. However, the dependence of these methods on image quality, i.e., noise, faint edges, etc, introduces a great deal of manual tuning for each image in order to obtain acceptable results.

DM methods use a template that deforms towards the boundaries or edges of vertebrae. In principle, DM is based on geometry, physics, and optimization theory [12]. Geometry is used to define and to keep track of the template at every step of the algorithm; physics is used to build the deformation rules so that information from the image deforms the template while shape restrictions keep it constrained; and optimization theory is used to build optimization functions that govern the evolution of the deformation and guarantee that it stops at the boundaries of the object of interest. Among the most representative works using DM to segment vertebrae are: the 3D topology-adaptive DM by McNerney and Terzopoulos [13]; the ellipsoidal DM used by Lipson *et al* to segment axial cross sections of vertebrae [14]; and the *snakes*-based [15] DM used by Gardner *et al.* to assess fractures in x-ray images [16]. The major shortcoming of DM methods is that their success largely depends on how well the template is initialized.

Statistical methods use *a priori* knowledge about the shape of the vertebrae. These methods employ a training set of images, i.e., a set of sample images, from which they extract shape and gray-level statistics. This information is used to build shape models. The objective is then to match the shape model to the information on target images. These methods are similar to DM because they allow a template to deform under the influence of external and internal forces. However, deformation is constrained by the statistics extracted from the training set. Among these methods, Cootes *et al* [17, 18, 19, 20, 21] proposed the technique of ASM for the automatic segmentation of objects. In ASM, shapes are defined by a set of landmark points (LPs) placed in corresponding positions of the object of interest on the training images. Smyth *et al* [17, 22] applied ASM on lumbar DEXA images for shape measurement. This system is semi-automatic because it requires three anchor points that constrain the movement of the model during deformation. Also, it was found that an ASM of several vertebrae is better than modeling one vertebra at a time. Accuracy was found to be comparable to inter-observer performance. In a slightly different application, Hutton, Cunningham, and Hammond [23] used ASM to locate cephalometric points in digitized lateral x-ray images of the head. Although the mean shape was manually placed close to the correct answer, just 74% of LPs ended up within 5mm of the expected location. Although this system was not found optimal for automatic operation, it was suggested that it could be used as a time saving tool for radiologists. Lorenz, and Krahnstöver [24] used a 3D statistical shape model for template fitting on CT images of lumbar vertebrae. This approach uses landmark-based training and Principal Component Analysis (PCA) to obtain the surface model. Then, it employs mesh deformation to *coat* a target object with the model. Here, manual intervention is required to place a reduced number of corresponding LPs in both the template and the object. After coating, a relaxation stage completes the deformation to capture fine detail and assure that LPs lie on the surface of the target object. This approach is semiautomatic and requires a prior segmentation of the target objects. Preliminary qualitative results showed good agreement with the manually segmented objects. Kohnen *et al.* [25, 26] employed ASM to segment hand radiographs with the purpose of determining bone maturity. In this approach, ASM is used to locate the main bones of the hand that serve as a guide to define regions of interest surrounding the bones. First, an *energy image* is built using edge extraction, distance between structures, and length of the contours. This energy image becomes the search space for ASM. The fitting process is optimized using simulated annealing based on the possible deformations of the mean shape. The same ASM algorithm was also applied to lumbar x-ray images obtaining acceptable results in 84% of the images [27].

ASM presents a number of shortcomings. First, as in the DM case, it requires an initialization step that places the model as close to the target object as possible. The problem is that most of the time this initialization is manual, i.e., a user has to interactively place the initial model on the target image. A second shortcoming is the assumption that shapes and gray-level values in the training set of images follow a specific distribution. The problem is that for some data sets this is not the case. In such instances, SM and GLM might be considered as invalid models because they fail to accurately represent the objects in the training set. The third shortcoming of ASM is that it performs global shape deformations, i.e., during deformation, the modeled shape follows the modes of variation of the training set. Therefore, local deformations are not allowed.

3.Methodology

The proposed segmentation algorithm consists of three modules, each one tailored to address one specific obstacle of the segmentation. The first module is a customized GHT algorithm that is used to find an estimate of vertebral pose within target images, i.e., GHT provides a global search technique. The second module is a customized version of ASM that is used to combine gray-level values and edge information in order to find vertebral boundaries. Here, ASM performs a gray-level match to the target images while keeping the generated shapes plausible. The third module is a customized DM approach based on the minimization of external and internal energies. Here, DM provides local deformation capabilities that allow the capture of fine details such as vertebral corners. The result of the integration of these three modules is a hierarchical approach in which GHT performs the first level of segmentation, i.e., the coarsest, and DM the last, i.e., the finest.

3.1. Data sets

The source of the images used in this work is the set of more than 17,000 x-ray images from the NHANES-II at NLM. Of these, 100 cervical and 100 lumbar images were chosen randomly to form the cervical and lumbar data sets, respectively. The size of the cervical images is 1463x1755 pixels and the size of the lumbar images is 2048x2487 pixels. Each image was digitized at 146dpi as part of the NHNES-II study [28].

3.2. Ground truth

Ground truth data is used to assess the performance of the segmentation algorithm in a quantitative fashion. For this work, ground truth is obtained from morphometric points that are placed by three expert radiologists. The protocol used to place these points is the one described under QM (Section 2). These morphometric points were used as the basis for placing the LPs that define the shapes for ASM and DM. For the cervical data set, 80 LPs define the shape of the vertebrae of interest, i.e., bottom endplate of C2 plus C3 through C6. For the lumbar data set, 200 LPs define the shapes of L1 through L5.

3.3. Tests and measurements

The proposed segmentation algorithm was applied to the cervical and lumbar data sets and segmentation results were obtained. Intermediate segmentation results at the output of each module, i.e., GHT, ASM, and DM, were obtained to verify that, at each step, a refinement on the segmentation took place. Segmentation error was measured quantitatively for each image in the data sets as the average Euclidean distance between the training LPs and the position of the LPs output by each segmentation step, and is given in millimeters as

$$error_{avg} = \frac{\sum_{i=1}^{nLP} \sqrt{(x_{train_i} - x_i)^2 + (y_{train_i} - y_i)^2}}{nLP}, \quad (1)$$

where nLP is the number of LPs in the shape, x_{train} and y_{train} are the coordinates of the training LPs, and x and y are the coordinates of the LPs given by the corresponding segmentation stage.

3.4. Customized GHT

GHT is used to obtain an estimate of vertebral pose, i.e., location, orientation, and scale, in target images. This estimate is necessary due to ASM's requirement of a proper initialization of the model in the target image. Therefore, GHT can be regarded as the first level of segmentation of the hierarchical approach. The motivation to use GHT is its ability to perform a global search for a shape template within a target image.

ASM's initialization shortcoming is due to the way ASM determines its initial pose. To determine its initial pose, ASM calculates the average pose of the shapes in the training set. It then uses this mean pose to initialize the mean shape. However, the assumption of a mean pose being enough for ASM initialization for the x-ray images used in this work is not a good one because subjects appear in a wide range of poses and this is a source of segmentation failure [11].

GHT addresses the issue of ASM initialization because its output is the pose of a shape template within a target image [29, 30]. We have shown that GHT can be customized to find vertebral pose in x-ray images [31]. However, the disadvantage of GHT is that the template is rigid, i.e., it is the same for all images and is not deformed throughout the searching process. For the present application, this feature renders GHT incapable of doing all the work of segmenting vertebrae because they present shape variations that cannot be captured by a rigid template. Therefore, at least one more step is necessary to capture vertebral shape faithfully and accurately, i.e., ASM.

For the cervical images, the GHT template represents the inferior endplate of C2 and C3 through C6, Figure 1a. For the lumbar images, the template represents L1 through L5, Figure 1b. To accommodate for the shape variation of the spine along our training sets of images, three templates for cervical vertebrae and three templates for lumbar vertebrae were constructed. One template represents the mean shape of the vertebrae and the other two represent the first mode of variation of the training set as calculated by PCA, Figure 2. In our preliminary experiments, it was found that two more matches of the templates on target images could exist. These matches represent the shift of the template along the spine. Due to the nature of GHT and the shape of the spine, it is not possible to ascertain which one of these matches represents the correct vertebrae depicted by the templates. Therefore, it was decided that the output of the customized GHT module would yield five values of pose, three corresponding to each template, and two corresponding to the shifts of the mean template along the spine. These values of pose are then processed by the next two modules, i.e., ASM and DM.

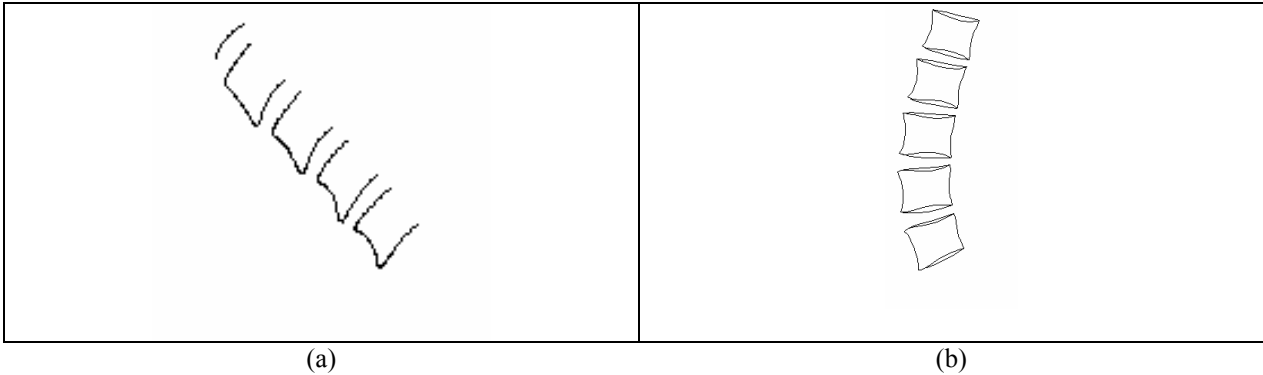


Figure 1. GHT template of (a) cervical vertebrae and (b) lumbar vertebrae.

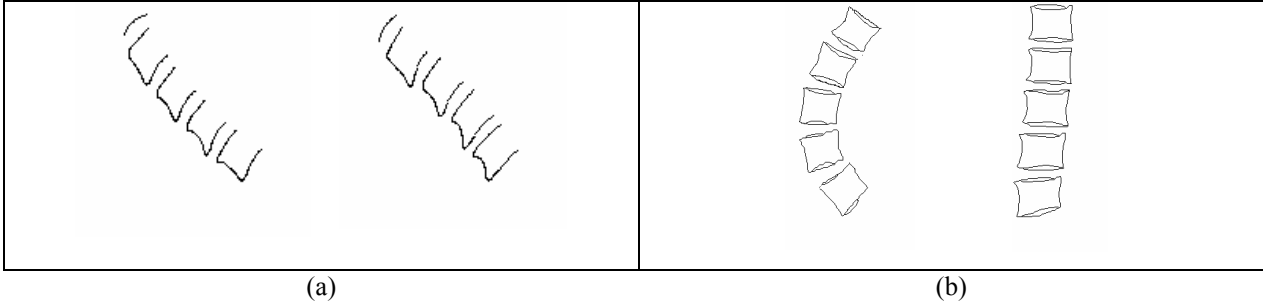


Figure 2. PCA templates of (a) cervical vertebrae and (b) lumbar vertebrae.

3.5. Customized ASM

The customized ASM module models shape and gray-level information from hand-annotated images and applies this knowledge to find evidence of the modeled objects in target images. The advantage of ASM is that the use of statistical information on shape and gray-level makes it, to some extent, insensitive to noise, occlusions, and faint boundaries. However, the original formulation of ASM has three shortcomings. First, it is very sensitive to the initialization of the model. Second, GLM relies on the representativeness of gray-level values in the model in order to find gray-level matches. Finally, ASM performs global shape deformations and is unable to allow local deformations. In the segmentation algorithm developed in this work, GHT addresses the initialization shortcoming and DM addresses the local deformation shortcoming. The remaining shortcoming, i.e., assuring GLM representativeness, is addressed by a custom implementation of ASM. Our implementation of ASM is based on the work described by Cootes *et al.* [17, 18, 19, 20, 21] but it has been customized for the application at hand. First, we have developed a methodology to analyze the ability of the main components of ASM, i.e., SM and GLM, to accurately capture the information from a training set of images [32]. With this methodology, we have found that, for the images in our training sets, SM can be considered as valid, i.e., it accurately represents the training set and is able to produce plausible shapes. However, we have also found that GLM, as built in the original formulation of ASM, is not a valid model, i.e., it is unable to accurately represent the variability of gray-level values at the boundaries of vertebrae. Therefore, we have developed a methodology to include edge information into GLM in such a way that the resulting model is a valid one.

3.5.1. SM analysis

In the original formulation of ASM, SM is built under the assumption that the distribution of shape parameters for each mode of variation follows a normal distribution. Under this assumption, constraints on shape parameters are set using multiples of the distribution's standard deviation. However, if the normality assumption is not correct for a training set of images, the SM built in this way might be considered invalid. Therefore, a methodology was developed to test the validity of SM for a specific training set of images [32]. This methodology is based on three steps. First, the assumption of normality is verified using the Mardia test of normality and the Kolmogorov-Smirnov goodness of fit test. Then, for those shape parameters that do not pass both tests, a *histogram specification* process redistributes the samples so that the resulting distribution is normal. In the third step, the original SM is compared to the modified SM in its ability to reproduce the shapes from the training set. If the difference in shapes is smaller than a predetermined threshold, then the original SM is deemed as a valid model. We have shown previously [32], that the images from our training sets produce a valid SM.

3.5.2. GLM analysis

In the original formulation of ASM, GLM is built under the assumption that it accurately represents the gray-level values across the boundaries of the vertebrae at the location of the LPs. If this not the case, then GLM might place the LPs on positions different than the target boundaries. We have developed a methodology to test for the representativeness of GLM with respect to a training set of images [32]. In this methodology, a *phantom* dataset is built from a reference image and is warped into the shapes that make up the training set. Then, GLMs for the original and phantom datasets are constructed. Finally, an *ideal search* experiment is performed, in which both GLMs are asked to locate the new position of LPs starting from their expected position for an image that is a part of the training set. Ideally, GLM should not move the LPs. If the movement of the LPs is, in average, larger than a predetermined threshold, using the GLM from the phantom GLM as reference, then the original GLM is deemed as invalid. We have shown previously [32], that the images from our training set produce an invalid GLM; therefore, a methodology to produce a valid GLM from the same set of images is required.

3.5.3. Edge blending

The purpose of adding edge information to GLM is to provide a certain level of uniqueness to the appearance of boundaries. In this way, GLM should be able to better localize them. The process to include edge information into GLM consists of two steps: edge extraction and blending. The first step, edge extraction, has been implemented with an empirical method that uses unsharp masking and thresholding, Figure 3. In this method, a Gaussian filter of size $[N \times N]$ and standard deviation σ enhances the edges and a hard threshold binarizes the image to keep only the edges. The edges are extracted for five different values of N and σ and are combined using an exclusive-or operation. The second step, edge blending, consists of combining the original gray-level image with its corresponding edge image. This task is

performed by averaging the two images as shown in Figure 4. A methodology to test the impact of this approach was developed. In this methodology, two GLMs were built. The first GLM was built using the original gray-level images from the cervical training set. The second GLM was built using the blended images corresponding to the images in the same training set. Then, an ideal search case was performed on both GLMs and the localization errors were recorded, Figure 5. It can be observed that localization errors from blended images are comparable to localization errors from the phantom dataset, which can be regarded as a reference set. This shows the relevance of using blended images.

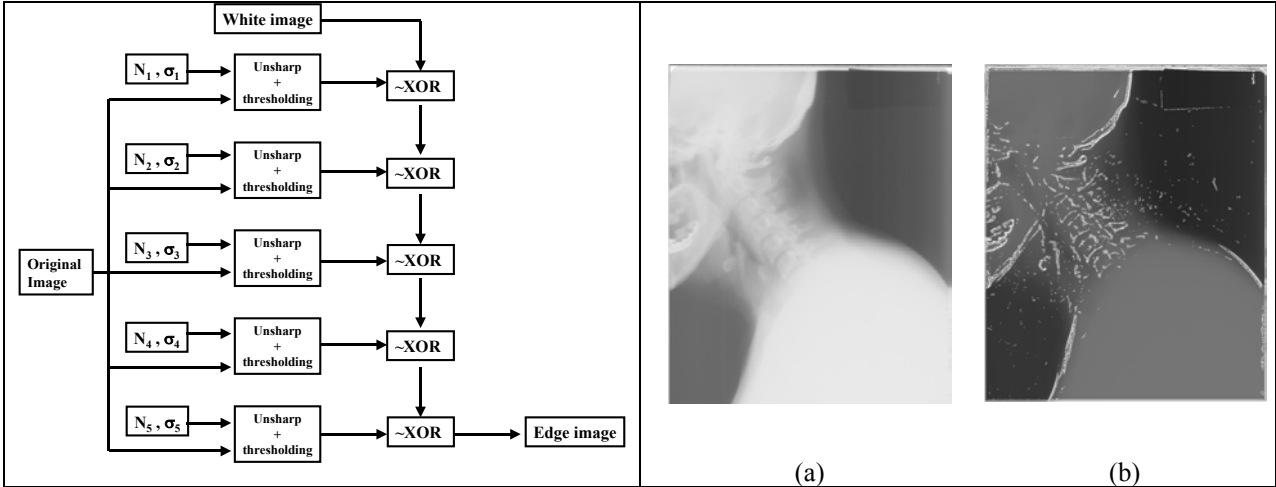


Figure 3. Algorithm to extract vertebral edges.

Figure 4. Sample of an (a) original and (b) corresponding blended image.

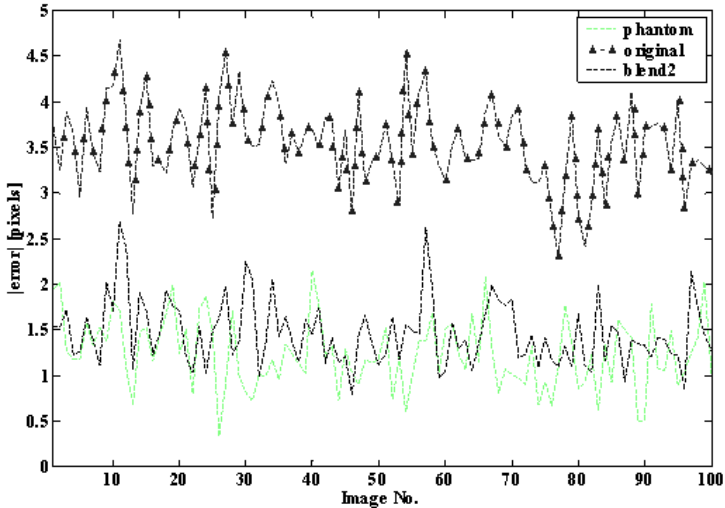


Figure 5. Results of an ideal search experiment for original, phantom, and blended GLMs.

3.6. Customized DM

The proposed customized implementation of DM is aimed at providing local deformations to capture fine details of vertebral boundaries at key points. The proposed DM formulation is based on the methodologies by Kass [15], Terzopoulos and Fleisher [33], and Tagare [34]. The customized DM in this work uses an energy minimization approach

to build an optimization function that, when minimized, yields the position of LPs at the edges of target images. This is done only at key positions of the vertebrae, i.e., it is a local DM. However, energy terms are not the same as those in the snakes formulation. Instead, external energy is extracted from the modeled gray-level values of the training images and data from the target images. Internal energy is a combination of two terms: smoothness and proximity to a reference template. Also, the search process is posed as minimizing a functional that can be solved using dynamic programming (DP) [34].

3.6.1. Energy minimization formulation

For a DM defined by n LPs, the energy functional has the form

$$\begin{aligned}
E(LP_1, LP_2, \dots, LP_n) = & \alpha_1 * \sum_{i=1}^n (g_{s_i} - \bar{g}_i) S_i^{-1} (g_{s_i} - \bar{g}_i) \\
& + \alpha_2 * \sum_{i=1}^n D(LP_i - LP_{ref_i}) \\
& + \alpha_3 * \sum_{i=1}^{n-1} |D(LP_i - LP_{ref_i}) - D(LP_{i+1} - LP_{ref_{i+1}})|,
\end{aligned} \tag{2}$$

where the first term of the right side of (2) is the external energy, the second term is the internal energy that represents proximity, and the third term is the internal energy that represents smoothness. The external energy term is derived from the optimization function of the GLM for each LP in the DM using the training set of images, where g_{s_i} is a testing profile of gray-level values at the current position of the i -th LP, \bar{g}_i is the mean profile of gray-level values for the i -th LP, and S_i^{-1} is the inverse of the covariance matrix of the training profiles of gray-level values. The first internal energy term represent the proximity of the current position of LPs to a reference template, where LP_i is the current position of the i -th LP, LP_{ref_i} is the position of the i -th reference LP, and $D()$ is the Euclidean distance operator.

3.6.2. Minimization via dynamic programming

The easiest way to optimize (1) is to evaluate the functional for every possible position of the LPs. However, this *brute force* approach is computationally intensive. Therefore, a different approach is needed. It can be shown [34], that (1) can be written as the sum of energy terms that depend on two consecutive LPs as

$$E(LP_1, LP_2, \dots, LP_n) = E(LP_1, LP_2) + E(LP_2, LP_3) + \dots + E(LP_{n-1}, LP_n). \tag{3}$$

The form of (3) lends itself for optimization via DP. DP reduces the computational complexity of (1) from $O(m^n)$, where m is the number of possible positions of each LP, to $O(m + (n-1)n^2)$ [35].

4. Results

This section presents the final segmentation results obtained with the proposed algorithm. Separate results for cervical and lumbar images are presented.

For each step of the segmentation, i.e., GHT, ASM, and DM, a histogram of segmentation errors was calculated. Figure 6a shows the histogram of the segmentation errors for GHT, ASM and DM for the cervical data set. In this histogram, the position of each bin represents a range of values for the segmentation errors, i.e., the average distance between segmented and actual vertebrae, and its size represents how many cases fell within that particular range. It can be seen

that, in 65 cases, the vertebrae with the pose calculated by GHT were within 3mm of the actual vertebrae. In the remaining 35 cases, the segmentation errors were bigger than 3mm. Then, in the next step of the segmentation, ASM was able to bring 10 more cases within 3mm of the actual vertebrae. However, DM was not able to bring more cases into this bin. A closer look at the first bin of Figure 6b (Figure 6b) shows in more detail that, in fact, DM was able to improve the segmentation in cases with errors around 2mm. The first bin in the histogram in Figure 6a represents the range of segmentation errors that can be considered as segmentation success. Therefore, the algorithm reached a 65% success rate in segmenting cervical vertebrae with GHT, 75% success rate with GHT+ASM, and 75% with GHT+ASM+DM. Figure 7 shows two examples of segmentation of cervical images.

Regarding the lumbar data set, Figure 8a shows the histogram of segmentation errors for GHT, ASM, and DM. In this case, it can be seen how ASM and DM improved the segmentation progressively. This can be noted by the increasing size of the first bin of the histogram from GHT to ASM and from ASM to DM. A closer look at the first bin of the histogram (Figure 8b) shows that these improvements occurred at the lowest values of error. As in the case of the cervical vertebrae, the first bin of the histogram in Figure 8a indicates the success rate of the segmentation algorithm. In this case, the success rate was 40% with GHT, 47% with GHT+ASM, and 49% with GHT+ASM+DM. Figure 9 shows two examples of segmentation of lumbar images.

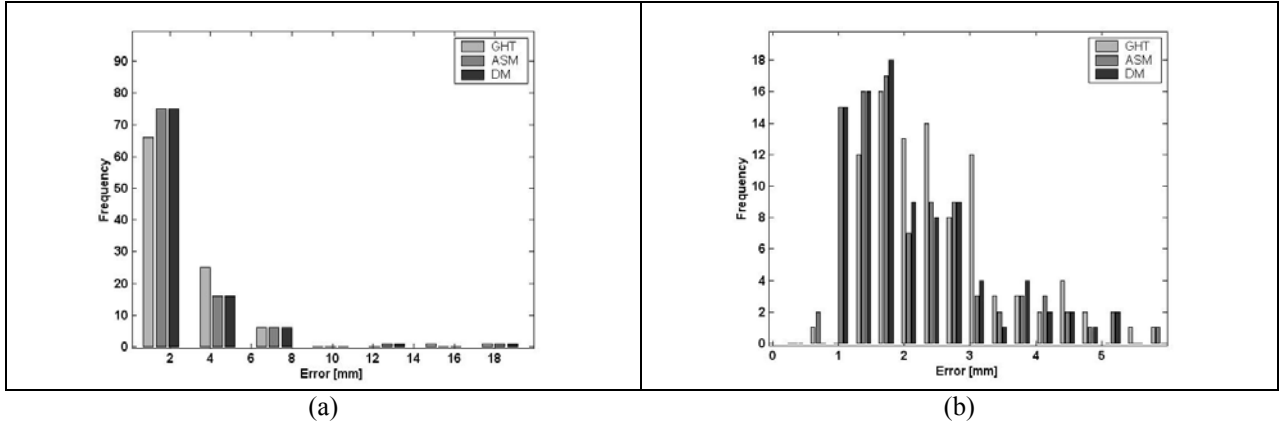


Figure 6. Histogram of segmentation errors for the cervical data set. (a) Full histogram, (b) and higher resolution histogram for the first bin.

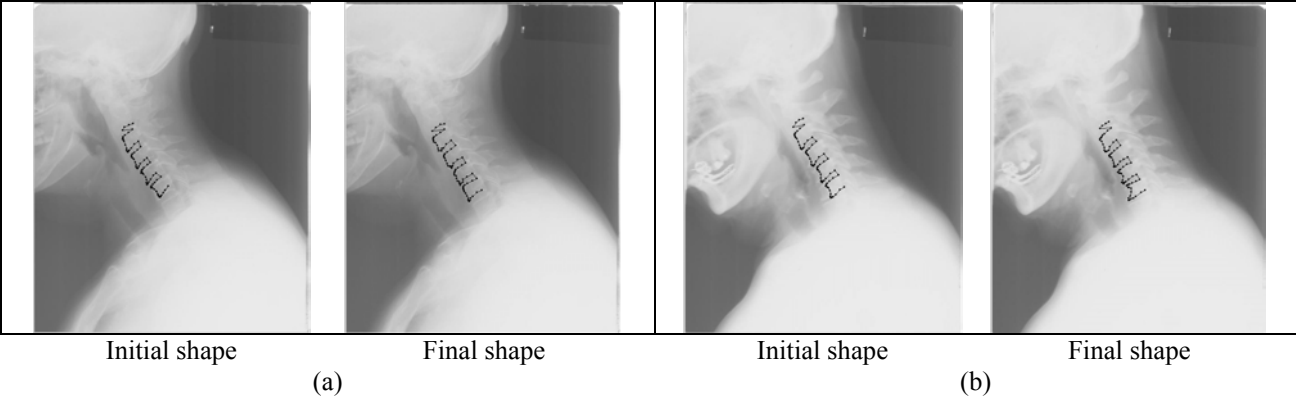


Figure 7. Examples of segmentation of cervical images. (a) error= 0.86mm, (b) error= 2.1mm.

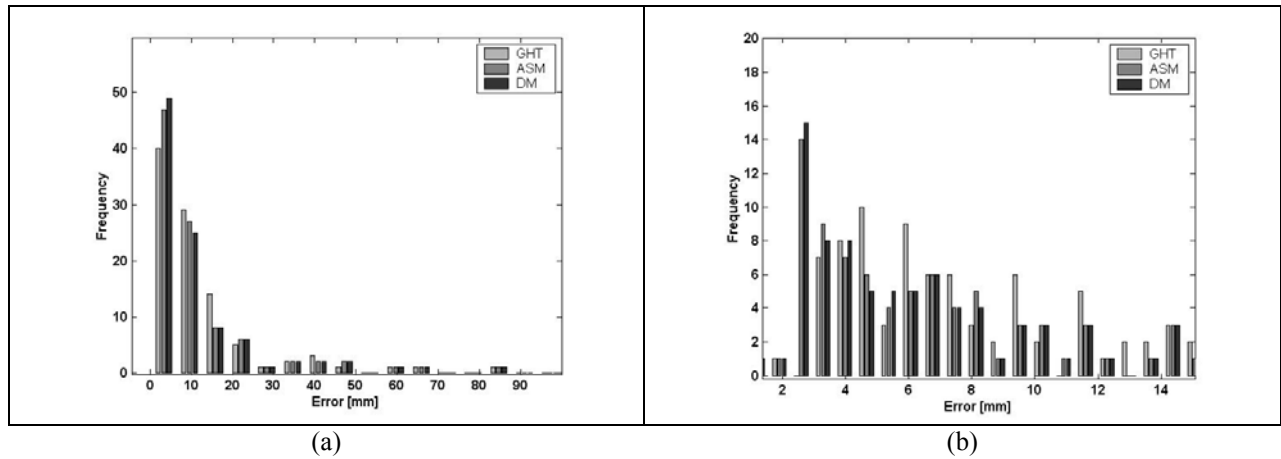


Figure 8. Histogram of segmentation errors for the lumbar data set. (a) Full histogram ;(b) and higher resolution histogram for the first bin.

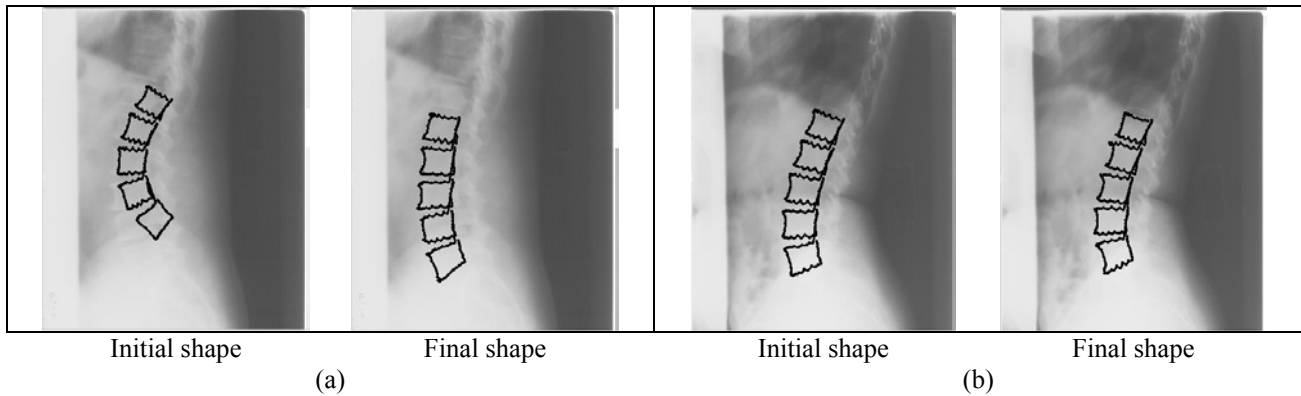


Figure 9. Examples of segmentation of lumbar images. (a) error= 5.18mm, (b) error= 2.27mm.

5. Conclusions

The problem of vertebrae segmentation in digitized x-ray images has been addressed with a hierarchical approach, which divides the process into three steps and each step performs an increasing level of segmentation from coarse to fine. Each one of these methodologies was studied and a number of feasibility experiments were designed to determine whether they could provide the results needed at each step of the segmentation. Each method was customized to accommodate the specific characteristics of vertebrae in x-ray images.

In our proposed approach, a customized GHT was used to estimate the pose of the vertebrae by matching a template that represents the vertebrae of interest to a target image. This estimate was used to initialize a customized ASM. From our analysis, the standard way to build SM yielded a valid model. However, GLM required the addition of edge information to yield a valid model. After segmentation with our customized ASM, DM provided local deformation at the anterior corners of vertebrae using an energy-minimization approach. The results of our experiments show that the proposed approach produces segmentation errors of less than 3mm in 75% of the cervical images and 6.4mm in 50% of the lumbar images.

ACKNOWLEDGEMENTS

This work was supported in part by the Communications Engineering Branch of the National Library of Medicine, Bethesda, MD 20894.

REFERENCES

1. J. A. Rea, M. B. Chen, J. Li, E. Potts, B. Fan, G. M. Blake, P. Steiger, I. G. Smith, H. K. Genant, I. Fogelman, "Morphometric X-ray Absorptiometry and Morphometric Radiography of the Spine: A Comparison of Analysis Precision and Osteoporotic Subjects," *Osteoporosis Int.* 9, 536-544 (1999).
2. J. A. Rea, M. B. Chen, J. Lin, G. M. Blake, P. Steiger, H. K. Genant, I. Fogelman, "Morphometric X-Ray Absorptiometry and Morphometric Radiography of the Spine: A Comparison of Prevalent Vertebral Deformity Identification," *J. Bone Miner. Res.* 15(3), 564-574 (2000).
3. V. M. Remes, M. T. Heinänen, J. S. Kinnunen, E. J. Marttinen, "Reference Values for Radiological Evaluation of Cervical Body Shape and Spinal Canal," *Pediatr. Radiol.* 30, 190-195 (2000).
4. National Library of Medicine, Digital Spine Atlas V1.0, July 11, 2002
<<http://archive.nlm.nih.gov/proj/atlas/index.php>>
5. H. K. Genant, M. Jergas, L. Palermo, M. Nevitt, R. San Valentin, D. Black, S. R. Cummings, "Comparison of Semiquantitative Visual and Quantitative Morphometric Assessment of Prevalent and Incident Vertebral Fractures in Osteoporosis," *J. Bone Miner. Res.* 11(7), 984-996 (1996).
6. M. P. Chwialkowski, P. E. Shile, D. Pfeifer, R. W. Parkey, R. M. Peshock, "Automated Localization and Identification of Lower Spinal Anatomy in Magnetic Resonance Images," *Comput. Biomed. Res.* 24, 99-117 (1991).
7. J. D. Helterbrand, R. E. Higgs Jr., P. W. Iversen, "Application of Automatic Image Segmentation to Tibiae and Vertebrae From Ovariectomized Rats," *Bone*, 21(5), 401-409 (1997).
8. M. Fiebich, C. M. Straus, V. Sehgal, "Image Processing- Automatic Bone Segmentation Technique for CT Angiographic Studies," *J. Comput. Assist. Tomo.* 23(1), 155-161 (1999).
9. L. R. Long, G. Thoma, "Segmentation and Image Navigation in Digitized Spine X-rays," *Medical Imaging 2000: Image Processing, Proc. SPIE* 3979, 169-175 (2000).
10. L. R. Long, G. Thoma, "Identification and Classification of Spine Vertebrae by Automated Methods," *Medical Imaging 2001: Image , Proc. SPIE* 4322, 1478-1479 (2001).
11. G. Zamora, H. Sari-Sarraf, S. Mitra, R. Long, "Estimation of Orientation and Position of Cervical Vertebrae for Segmentation with Active Shape Models," *Medical Imaging 2001: Image Processing, Proc. SPIE* 4322, 378-387 (2000).
12. T. McInerney, D. Terzopoulos, "Deformable Models in Medical Image Analysis: A Survey," *Med. Image Anal.* 1(2), 91-108 (1996).
13. T. McInerney, D. Terzopoulos, "Topology Adaptive Deformable Surfaces for Medical Image Volume Segmentation," *IEEE T. Med. Imaging* 18(10), 840-850 (1999).
14. P. Lipson, A. L. Yuille, D. O'Keefe, J. Cavanaugh, J. Taaffe, D. Rosenthal, "Deformable Templates for Feature Extraction from Medical Images," *First European Conference on Computer Vision, Lecture Notes Comput. Sc.* 427, 477-484 (1990).
15. M. Kass, A. Witking, D. Terzopoulos, "Snakes: Active Contour Models," *Int. J. Comput. Vision*, 1(4), 321-331 (1988).
16. J. C. Gardner, S. L. Heyano, L. G. Yaffe, G. von Ingersleben, C. H. Chesnut III, "A Semi-automated Computerized System for Fracture Assessment of Spine X-ray Films," *Medical Imaging 1996: Image Processing, Proc. SPIE* 2710, 996-1008 (1996).
17. T. F. Cootes, C. J. Taylor. Statistical Models of Appearance for Computer Vision. Home page. October 26, 2001. <<http://www.isbe.man.ac.uk/~bim/>>
18. A. Hill, T. F. Cootes, C. J. Taylor, K. Lindley, "Medical Image Interpretation: A Generic Approach using Deformable Templates," *Med. Inform.* 19(1), 47-59 (1994).
19. A. Hill, T. F. Cootes, C. J. Taylor, "Active Shape Models and the Shape Approximation Problem," *Image Vision Comput.* 14, 601-607 (1996).
20. C. J. Taylor, T. F. Cootes, A. Lanitis, G. Edwards, P. Smyth, A. D. W. Kotcheff, "Model-based Interpretation of Complex and Variable Images," *Philos. T. Roy. Soc. B* 352, 1267-1274 (1997).

21. T. F. Cootes, C. J. Taylor, "Statistical Models of Appearance for Medical Image Analysis and Computer Vision," *Medical Imaging 2001: Image Processing, Proc. SPIE* 4322,236-248 (2001).
22. P. P. Smyth, C. J. Taylor, J. E. Adams, "Vertebral Shape: Automatic Measurement with Active Shape Models," *Radiology* 211, 571-578 (1999).
23. T. J. Hutton, S. Cunningham, P. Hammond, "An Evaluation of Active Shape Models for the Automatic Identification of Cephalometric Landmarks," *Eur. J. Orthodont.* 22(5), 499-508 (2000).
24. C. Lorenz, N. Krahnstöver, "Generation of Point-Based 3D Statistical Shape Models for Anatomical Objects," *Comput. Vis. Image Und.* 77(2), 175-191 (2000).
25. M. Kohnen, F. Vogelsang, B. B. Wein, M. Kilbinger, R. W. Günther, F. Weiler, J. Bredno, J. Dahmen, "Knowledge Based Automated Feature Extraction to Categorize Secondary Digitized Radiographs," *Medical Imaging 2000: Image Processing, Proc. SPIE* 3979, 709-717 (2000).
26. F. Vogelsang, M. Kohnen, H. Schneider, F. Weiler, M. W. Kilbinger, B. B. Wein, R. W. Günther, "Skeletal Maturity Determination from Hand Radiograph by Model Based Analysis," *Medical Imaging 2000: Image Processing, Proc. SPIE* 3979, 294-305 (2000).
27. M. Kohnen, A. H. Mahnken, A. S. Brandt, S. Steinberg, R. W. Günther, B. B. Wein, "Segmentation of the Lumbar Spine with Knowledge Based Shape Models," *Medical Imaging 2002: Image Processing, Proc. SPIE* 4684, 1578-15872 (2002).
28. National Library of Medicine, NHANES II X-ray images, May 1st, 2001
<<http://archive.nlm.nih.gov/proj/ftp/ftp.php>>.
29. D. H. Ballard, "Generalizing the Hough Transform to Detect Arbitrary Shapes," *Pattern Recogn.* 13(2), 111-122 (1981).
30. V. F. Leavers, "Which Hough Transform?," *Image Und.* 58(2), 250-264 (1993).
31. A. Tezmol, H. Sari-Sarraf, S. Mitra, R. Long, "Customized Hough Transform for Robust Segmentation of the Cervical Vertebrae from X-Ray Images," *SSIAI 2002, Proc. IEEE* 1537, 224-228 (2002).
32. G. Zamora, H. Sari-Sarraf, S. Mitra, R. Long, "Analysis of the Feasibility of Using Active Shape Models for Segmentation of Gray Scale Images," *Medical Imaging 2002: Image Processing, Proc. SPIE* 4684, 1370-1381 (2002).
33. D. Terzopoulos, K. Fleischer, "Deformable Models," *Visual Comput.* 4(6), 306-331 (1988).
34. H. D. Tagare, "Deformable 2-D Template Matching Using Orthogonal Curves," *IEEE T. Med. Imaging*, 16(1), 108-117, (1997).
35. D. H. Ballard, C. M. Brown, *Computer Vision*, Prentice-Hall, Englewood Cliffs, NJ, 137-143 (1982).